J-matrix calculation of electron-helium S-wave scattering. II. Beyond the frozen-core model

Dmitry A. Konovalov
ARC Centre for Antimatter-Matter Studies and
Discipline of Information Technology, School of Business,
James Cook University, Townsville, Queensland 4811, Australia

Dmitry V. Fursa and Igor Bray
ARC Centre for Antimatter-Matter Studies, Curtin University,
GPO Box U1987, Perth, Western Australia 6845, Australia

(Dated: September 12, 2012)

In the preceding J-matrix (JM) paper [D. A. Konovalov *et. al.* Phys. Rev. A **84**, 032707 (2011)], the S-wave e-He scattering (S-e-He) problem was solved within the frozen-core (FC) model of helium for impact energies in the range 0.1-1000eV. In this sequel, both target electrons are described within the configuration-interaction model of helium obtaining more accurate (compared to the FC model) first seven bound states of the S-wave helium. The presented JM calculations are ~~essentially exact~~ numerical solution of the S-e-He problem for the ~~total~~ elastic, $2^{1,3}S$, $3^{1,3}S$ excitation cross sections ~~below the ionization threshold~~. The JM results are confirmed by the corresponding convergent-close-coupling (CCC) calculations creating a challenging benchmark for any current or future *ab initio* electron-atom scattering methods.

~~Above the ionization threshold, only the elastic, triplet 2^3S excitation and ionization cross sections are obtained at the benchmark accuracy level. The rest of excitation cross sections still exhibit noticeable pseudo-resonances (up to 10% fluctuations), which could not be eliminated with the considered number of target states (up to 95 eigenstates of He were considered).~~

PACS numbers: 34.80.Dp

I. INTRODUCTION

This study focuses on the S-wave e-He (S-e-He) scattering model, where the target helium atom is in its ground state before the electron impact, and where only the partial wave with zero angular momentum ($l = 0$) is retained in all calculations and partial-wave expansions. The S-wave models have proven to be a very productive testing ground for *ab initio* scattering theories, see [1–18] for the S-wave e-H scattering (S-e-H) and [19–27] for the S-e-He problem. The main attraction of the S-wave models is that they retain most of the physics complexities of the full scattering problems while reduce the problems computationally. Furthermore it is somewhat expected that if a theoretical method solves a S-wave model, then the remaining partial waves could be solved with additional computational resources, see for example the convergent-close-coupling (CCC) [28], R-matrix (RM) [29–31] and J-matrix (JM) [32, 33] methods.

The main goal of this study is to provide high accuracy S-e-He cross sections highlighting resonant features of the cross sections where applicable. The need for such benchmark calculations is evident from the existing *ab initio* attempts to solve the S-e-He problem. Reviewing in reverse chronological order, in 2010, Bartlett and Stelbovics [25] developed a four-body propagating exterior scaling (PECS) method and reported results claiming to achieve "benchmark" level of accuracy. However none of their cross sections, including elastic and $2^{1,3}S$ excitation cross sections, displayed resonances at the accuracy level achieved for the S-e-H problem [3]. In 2005, Horner et al. [24] reported results using time-dependent exterior complex scaling (TD-ECS), which also failed to described resonance behavior of the cross sections. In 2002 and 2004, the CCC method [21, 22] did not examine the resonance regions with sufficiently fine energy grid. This is now corrected to some extent when in 2011 Konovalov et al. [27] reported the CCC and JM *frozen-core* (FC) results clearly showing the resonances in the elastic and $n = 2$ (2^1S and 2^3S) excitation cross sections. The RM method [29, 31] has never reported its results for the S-e-He problem. In summary, while the three most recent methods (PECS, TD-ECS, CCC) are in good qualitative or overall agreement with each other, in many specific cases their results differ by as much as 10-20% [24, 25]. These discrepancies together with the failure to describe the resonance features of the model, is a major theoretical gap as far as the scattering theory is concerned.

The stated goal is attempted and achieved in many aspects by combining advantages of the CCC and JM methods, where the later has been recently revised [27] by merging it with the Fano's multi-configuration interaction matrix elements [34]. The CCC method is able to solve the scattering problem very accurately via the Lippmann-Schwinger equation [35]. However, it is not practical to run the CCC method for each of the many thousands of impact energy points required for the final benchmark results. On the other hand, the JM method is very efficient [36, 37] in calculating a vast number of energy points but numerical-convergence properties of the

JM method remains largely unknown. The JM and CCC methods are implemented independently and use completely different approaches to solve the scattering equations. Therefore, the CCC and JM methods can be and were used to cross-verify that their results are convergent within their own numerical parameters at key energy points. See [38] for information on availability of the results and source code.

TABLE I: Energy levels (a.u.) and excitation thresholds (eV) of the first nine bound states of helium in the S-wave model.

Classification	threshold (eV)	Eigenvalues (a.u)	(N_c,N_t)
He($1s^2$,^1S)	0	-2.879 028 569 1	(50,50)
error =	0.001 80	-2.878 962 303	(7,30)
error =	0.015 94	-2.878 442 699	(3,30)
error =	0.177 47	-2.872 506 673	(1,30)
He($1s2s$,^3S)	19.178	-2.174 264 856 3	(50,50)
		-2.174 264 618	(7,30)
		-2.174 245 504	(1,30)
He($1s2s$,^1S)	19.996	-2.144 197 258 7	(50,50)
		-2.144 191 393	(7,30)
		-2.143 449 321	(1,30)
He($1s3s$,^3S)	22.056	-2.068 490 070	(7,30)
		-2.068 484 660	(1,30)
He($1s3s$,^1S)	22.266	-2.060 792 356	(7,30)
		-2.060 573 161	(1,30)
He($1s4s$,^3S)	22.928	-2.036 438 560	(7,30)
		-2.036 436 372	(1,30)
He($1s4s$,^1S)	23.011	-2.033 392 203	(7,30)
		-2.033 300 706	(1,30)
He($1s5s$,^3S)	23.305	-2.022 583 695	(7,30)
		-2.022 582 608	(1,30)
He($1s5s$,^1S)	23.346	-2.021 079 423	(7,30)
		-2.021 033 007	(1,30)
$He^+(1s)$	23.920	-2	Ionization

II. THEORY

The JM method [36, 37] is a very general method for solving wide range of scattering problems. In this study, we continue to develop the version of the JM method that was previously applied to the S-e-H [39] and S-e-He [27] scattering problems. Hereafter this version will be referred to as the KFB method to assist when discussing its features which are not necessarily part of the generic JM method.

When the KFB method was applied to the FC model of helium [27] (one electron was always in the $1s$ state of He^+), the following three sets of functions were used: target basis, JM functions, and Laguerre basis.

Target basis is a set of N_t orthonormal radial functions $\{P_n(r)\}_{n=1}^{N_t}$, where $P_n(r)$ is used as the radial component of the n'th subshell wave function when building one- or many-electron wave functions as per the Fano's procedure [27, 34].

JM functions are the nonorthogonal Laguerre functions $\{\xi_p(r)\}_{p=0}^{\infty}$ from the original JM method [36, 37],

$$\xi_p(r) = x^{l+1}\mathrm{e}^{-x/2}L_p^{2l+1}(x), \quad p = 0, 1, ..., \infty, \tag{1}$$

where $x = \lambda r$, λ is Laguerre exponential falloff, $l \equiv 0$ (for the S-model), and $L_p^{\alpha}(x)$ are the associated Laguerre polynomials [40].

Laguerre basis is the set of orthonormal Laguerre functions $\{R_p(r)\}_{p=0}^{\infty}$,

$$R_p(r) = C_p x^{l+1}\mathrm{e}^{-x/2}L_p^{2l+2}(x), \quad p = 0, 1, ..., \infty, \tag{2}$$

$$\int_0^{\infty} dr\ R_p(r)R_{p'}(r) = \delta_{pp'},\ C_p = \sqrt{\frac{\lambda p!}{(p+2l+2)!}}. \tag{3}$$

Note that for any fixed N_t, both $\{\xi_p(r)\}_{p=0}^{N_t}$ and $\{R_p(r)\}_{p=0}^{N_t}$ span identical functional space [39].

The target basis $\{P_n(r)\}_{n=1}^{N_t}$ is selected or built by diagonalizing a suitable one-electron Hamiltonian [27, 39]. Then, the two-electron target-helium wave functions are constructed by allowing first and second helium electrons to occupy the first N_c and N_t radial functions, respectively, where N_c controls the number of allowed *core* excitations with $N_c = 1$ being the frozen-core model.

After many numerical experiments, it became apparent that the core excitation functions $\{P_n(r)\}_{n=1}^{N_c}$ should be constructed differently from the rest of the target basis $\{P_n(r)\}_{n=N_c+1}^{N_t}$. Otherwise, the convergence by N_c is just too slow to be computationally practical. This is due to the two very different radial scales present in this study. The short-range core excitations are essentially adjustments to the $1s$-orbital of He^+. While the helium excitations below the ionization threshold resemble ns-orbitals of hydrogen and therefore are long-range. This problem is solved here by using a mix of the short range $\{R_p^c(r)\}_{p=0}^{N_c-1}$ with $\lambda_c = 4$ and long-range $\{R_p^t(r)\}_{p=N_c}^{N_t-1}$ with $\lambda_t = 1$ basis sets when constructing the target basis as follows.

The JM method splits the one-electron radial functional space into *inner* $\{\xi_p\}_{p=0}^{N-1}$ and *outer* $\{\xi_p\}_{p=N}^{\infty}$ subsets controlled by the number N of JM functions in the inner subset [36, 37]. In the KFB method, the target basis $\{P_n(r)\}_{n=1}^{N_t}$ must be orthogonal to the outer JM functions $\{\xi_p\}_{p=N}^{\infty}$, where $N_t < N$. Let $\lambda \equiv \lambda_t$ and $\hat{I}_t$ be a projection operator into the functional space of $\{R_p^t(r)\}_{p=0}^{N_t-1}$

$$\hat{I}_t = \sum_{p=0}^{N_t-1} |R_p^t\rangle\langle R_p^t|, \tag{4}$$

then by construction every function from $\{R_p^t(r)\}_{p=0}^{N_t-1}$ and $\{R_p^{ct}(r)\}_{p=0}^{N_c-1}$

$$R_p^{ct} = \hat{I}_t R_p^c, \tag{5}$$

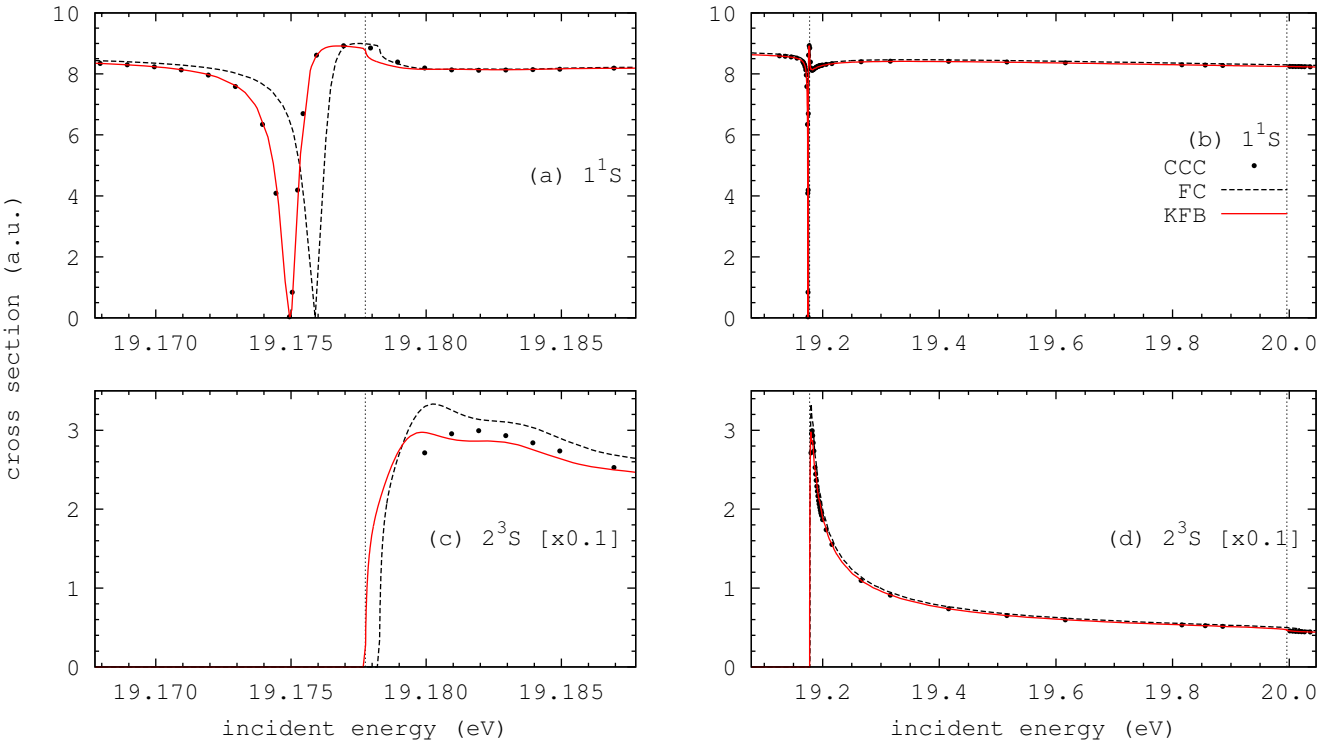

FIG. 1: (Color online) Elastic (1^1S) and 2^3S single-excitation e-He S-wave cross sections between and around 2^3S and 2^1S thresholds shown by vertical dashed lines. Sub-figures (a) and (c) zoom in on the 2^3S excitation threshold (Table I). FC (Frozen-core, $N_c = 1$, $N_t = 30$), KFB ($N_c = 7$, $N_t = 30$) and CCC ($N_c = 3$, $N_t = 30$) results were shifted to the right by 0.17747eV, 0.0018eV and 0.01594eV (Table I), respectively.

is orthogonal the outer JM functions. The final target basis $\{P_n(r)\}_{n=1}^{N_t}$ is constructed by making a single orthonormal basis from $\{R_p^{ct}(r)\}_{p=0}^{N_c-1}$ and $\{R_p^t(r)\}_{p=N_c}^{N_t-1}$ via the Gram-Schmidt process. Note that in the CCC method the final target basis $\{P_n^{3C}(r)\}_{n=1}^{N_t}$ is also built via the Gram-Schmidt process but from $\{R_p^c(r)\}_{p=0}^{N_c-1}$ and $\{R_p^t(r)\}_{p=N_c}^{N_t-1}$ sets, that is, the intermediate R_p^{ct} functions were not required.

III. RESULTS AND DISCUSSION

See Supplemental Material at [URL will be inserted by publisher] for the results in tabular form.

The number N is the key JM parameter responsible for the convergence of any implementation of the JM method. That is, the larger the N, the more accurate the corresponding JM results are expected to be. Within the current KFB method, maximum value of N is limited to around 100 so that the method remains to be easily accessible to wider research community. All presented in this study KFB results were still calculated on a consumer-grade laptop.

The following KFB computational parameters were used, see [39] for explanation of the parameters: $\lambda_c = 4$, $\lambda_t = 1$, $N_t = 30$, $N = 100$, $\ln(c) = -5 - 2\ln(Z_{\rm He})$, $Z_{\rm He} = 2$, $r_{\rm max} = 500$, $M_{LCR} = 2001$, where the radial grid was between zero and $r_{\rm max}$, and M_{LCR} is the number of equally spaced points in the radial LCR grid [39].

The two-electron configurations (in both KFB and CCC methods) are constructed by occupying radial subshells $\{P_n(r)\}_{n=1}^{N_t}$ with all spin-permitted (n_1s, n_2s) and $(1s, n_2's)$ configurations, where $1 \le n_1 \le n_2 \le N_c$ and $N_c < n_2' \le N_t$. The three-electron configurations in the KFB method are built by adding an extra n_3s-electron with $n_2 \le n_3 \le N$ or $n_2' \le n_3 \le N$ to each of the available two-electron configurations and keeping only the ones that are permitted by the Pauli exclusion principle and spin-coupling rules.

Hereafter FC, KFB and CCC denote results obtained with $N_c = 1$, $N_c = 7$ and $N_c = 3$, respectively. The ($N_c = 7$, $N_t = 30$, $N = 100$)-combination yields 51 singlet (^1S) and 44 triplet (^3S) eigenstates of helium, and 8418 eigenstates of $He^-(^2S)$. When converting to eV scale, 27.2116 eV was used as the atomic unit of energy (or Hartree).

Table I shows first nine eigenvalues from diagonalizations of S-wave helium Hamiltonian. Selecting $\lambda_c = 4$ creates the first target radial function $P_1(r)$ numerically identical to the exact $1s$ state of He^+, when N_t is sufficiently large as is the case for the used $N_t = 30$. The main improvement of the $N_c = 7$ basis over the froze-core case ($N_c = 1$) is in the ground state of helium, where the

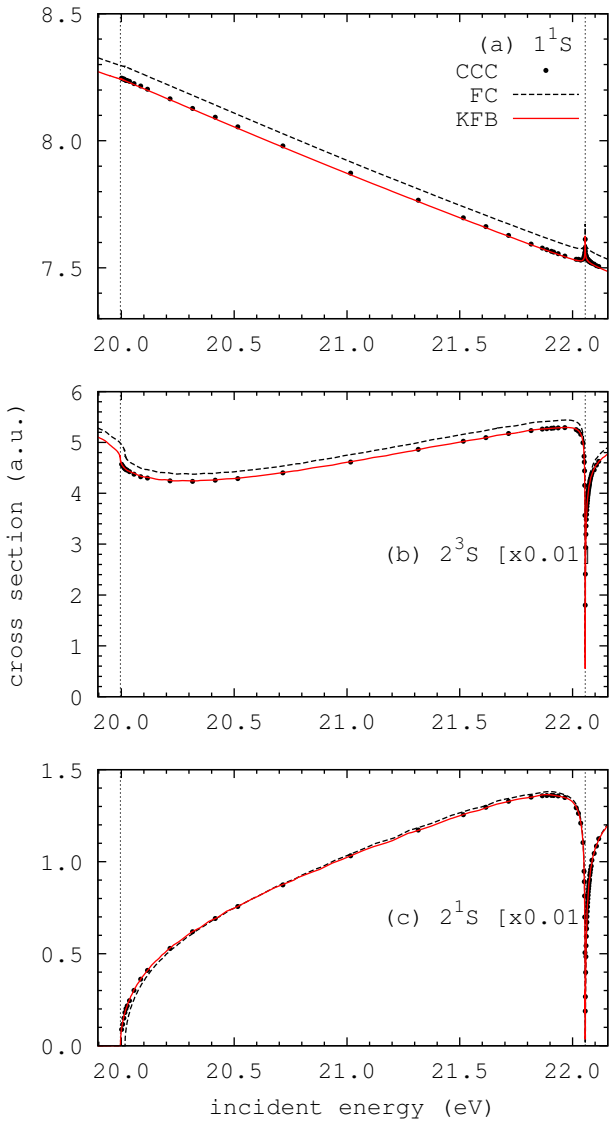

FIG. 2: (Color online) The same as in Fig. 1 but with added 2^1S excitation cross section, and for incident energies between and around 2^1S and 3^3S thresholds shown by vertical dashed lines.

first seven significant digits [41] were obtained by using $\{R_p^c(r)\}_{p=0}^{N_c-1}$ as the basis for both electrons with $N_c = 50$ and $\lambda_c = 4$, denoted by $(50, 50)$ in Table I.

Figs. 1-5 show nearly exact agreement between the KFB and CCC methods yielding two important conclusions. First, it confirms that the KFB results are convergent by N when solving the scattering equations via the JM method. Second, both CCC and KFB are convergent by the number of core excitations N_c, where KFB used $N_c = 7$ and CCC used $N_c = 3$ in Figs. 1-4.

Figs. 1-4 show that if the FC results are shifted (as they are on the figures) to the right by the FC ground energy error (0.17747eV, see Table I), the FC and KFB results become very close. This means that most of the S-wave scattering dynamics is essentially due to the movement of one electron in the field of $1s$ state of He^+. In most cases, the full KFB results differ from the FC results by no more than 10% (after the shift).

Figs. 1(a) and 1(c) zoom in onto the negative-ion resonance $He^-(1s(2s)^2,^2S)$ that exists just below and within 5meV of the 2^3S-excitation threshold. Again, the FC model fully explains the results, while the KFB model provides the final adjustments to arrive at the benchmark solution in Figs. 1(a), 1(b), and 1(d). Fig. 1(c) exposes the challenging energy region (about 5meV) just above the 2^3S excitation threshold, where the CCC and KFB results are comparable but slightly different and therefore only the CCC results should be considered as the benchmark solution in this particular case. Note that the very sharp peak (Fig. 1c) disappears in the real e-He scattering [33, 42] as the $He^-(19.3eV)$ resonance [43–45] lies too far away from the 2^3S(19.7eV) excitation threshold [42].

Figs. 2(c) and 4(d) show that the 2^1S and 3^1S singlet excitations do not have the resonant behavior at thresholds. Hence $He^-(^2S)$-states are absent near the singlet thresholds in the S-wave model. Again this is different from the full model, where such $He^-(^2S)$-states do exist yielding sharp peaks in the 2^1S [33, 42] and 3^1S [31] near-threshold cross sections.

Fig. 3 reveals very feature-rich behavior around the triplet 3^3S excitation threshold. A He^- metastable state exists immediately near (within 1meV) the 3^3S excitation threshold causing the very sharp peak of the 3^3S and very sharp dips in the $n = 2$ cross sections at the threshold. Note particularly interesting Fig. 3(e), which could only be obtained within KFB when both N_t and N are sufficiently large. The TEST ($N_c = 1$, $N_t = 20$, $N = 21$) line in Fig. 3(e) clearly shows how the resonance behavior is very sensitive to the quality of the relevant He^- metastable wave function.

Fig. 4 shows rich interplay of cross sections between the 3^1S and ionization thresholds, where the $He^-(^2S)$ resonances exist near the corresponding triplet 4^3S-7^3S helium states. The resonance peak/dip amplitudes are diminishing with n and become indistinguishable above 7^3S, where the helium eigenstates become progressively less accurate in describing the helium bound states with higher n.

Above the ionization threshold (Fig. 5) both KFB and CCC exhibit pseudo-resonances. Pseudo-resonances depend strongly on particular basis parameters, where in this case the parameters are N_c, $\lambda_c = 4$, N_t and $\lambda_t = 1$. An attempt is made to exploit this property by running KFB method multiple times with $N_c = 3$ and $25 \le N_t \le 35$ and then average the results, see line AVR in Fig. 5. This technique is arguable justified by considering that the true resonances will remain unaffected by this averaging if the calculation parameters are varied with the convergent range. The AVR method worked spectacularly well for the total ionization cross section (TICS in Fig. 5b), where the AVR results are proposed to be the correct benchmark solution. Surpris-

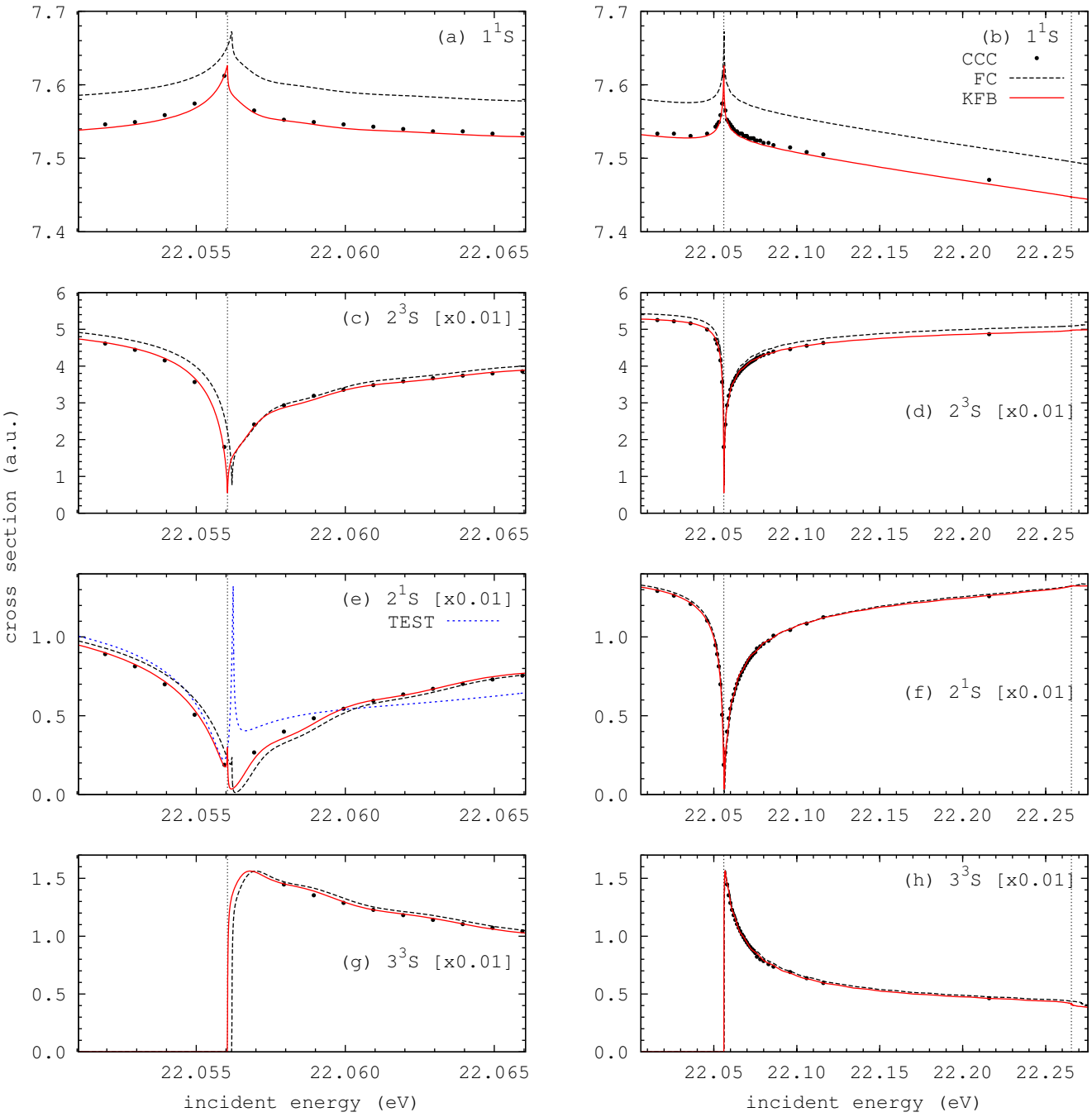

FIG. 3: (Color online) The same as in Fig. 2 but with added 3^3S excitation cross section, and between and around the 3^3S and 3^1S thresholds shown by vertical dashed lines. Sub-figures (a), (c), (e) and (g) zoom in on the 3^3S excitation threshold (Table I). TEST denotes the KFB calculation with $N_c = 1$, $N_t = 20$ and $N = 21$.

ingly, the 2^1S (Fig. 5d) and $n = 3$ (Figs. 5e and 5f) AVR results revealed a set of highly persistent pseudo-resonances around 30eV. Therefore, it is proposed that the AVR results (above the ionization threshold) approximate the correct benchmark solution within the error bar given by the remaining non-physical oscillations.

IV. CONCLUSIONS

TODO

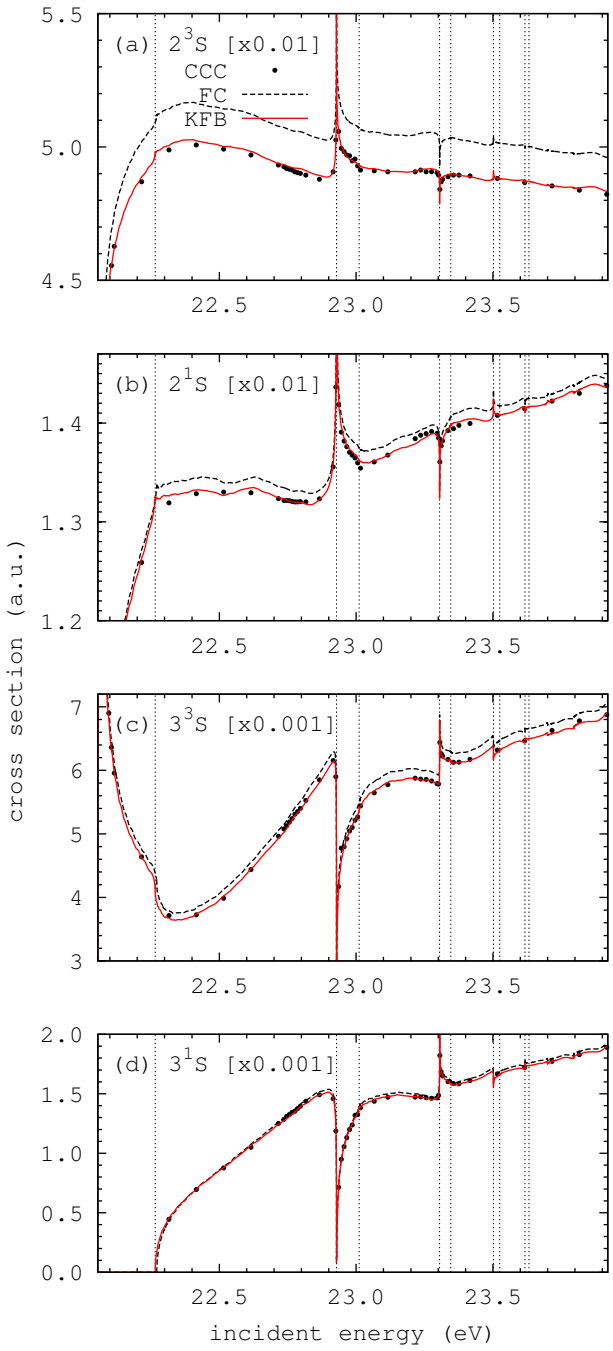

FIG. 4: (Color online) The same as in Fig. 3 but with added 3^1S excitation cross section between the 3^3S and ionization thresholds (23.92eV, Table I). The 3^1S, $4^{3,1}S$, ..., $7^{3,1}S$ excitation thresholds (Table I) are shown by vertical dashed lines (from left to right).

Acknowledgments

This work was supported by the Australian Research Council. IB acknowledges the Australian National Computational Infrastructure Facility and its Western Australian node iVEC.

[1] A. Temkin, Phys. Rev. **126**, 130 (1962).
[2] E. J. Heller and H. A. Yamani, Phys. Rev. A **9**, 1209 (1974).
[3] R. Poet, J. Phys. B **11**, 3081 (1978).
[4] R. Poet, J. Phys. B **13**, 2995 (1980).
[5] R. Poet, J. Phys. B **14**, 91 (1981).
[6] J. Callaway and D. H. Oza, Phys. Rev. A **29**, 2416 (1984).
[7] I. Bray and A. T. Stelbovics, Phys. Rev. Lett. **69**, 53

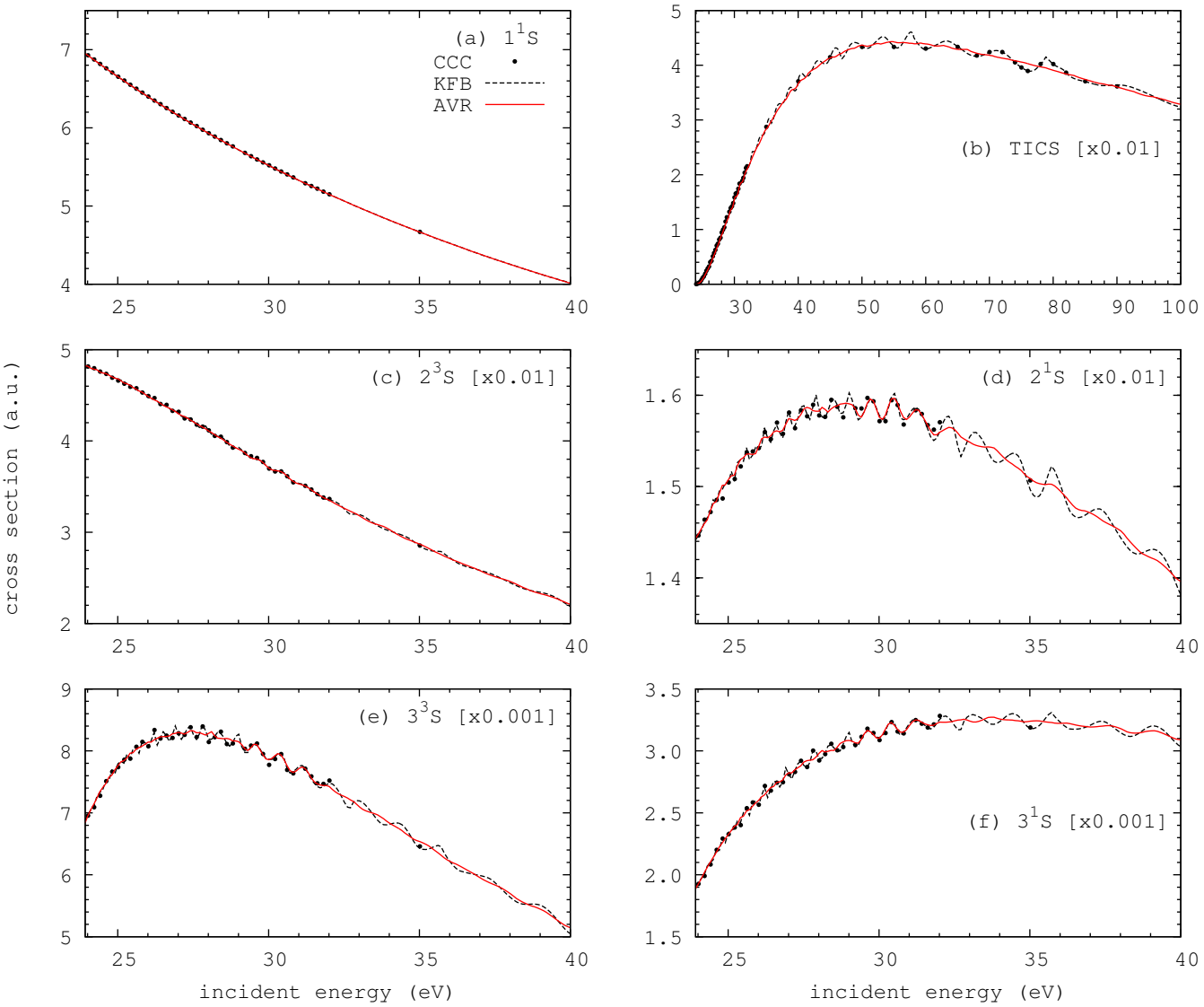

FIG. 5: (Color online) The same as in Fig. 4 but with added total ionization cross section (TICS) for incident energies above the ionization threshold. AVR denotes averaged KFB calculations with $N_c = 3$, $25 \leq N_t \leq 35$ and $N = 100$. Note that in this figure all results are not corrected for the ground energy errors (curves are not shifted).

(1992).
[8] A. K. Bhatia, B. I. Schneider, and A. Temkin, Phys. Rev. Lett. **70**, 1936 (1993).
[9] D. A. Konovalov and I. E. McCarthy, J. Phys. B **27**, L407 (1994).
[10] W. Ihra, M. Draeger, G. Handke, and H. Friedrich, Phys. Rev. A **52**, 3752 (1995).
[11] M. S. Pindzola and D. R. Schultz, Phys. Rev. A **53**, 1525 (1996).
[12] S. Jones and A. T. Stelbovics, Phys. Rev. A **66**, 032717 (2002).
[13] S. Jones and A. T. Stelbovics, Phys. Rev. Lett. **84**, 1878 (2000).
[14] M. Baertschy, T. N. Rescigno, W. A. Isaacs, and C. W. McCurdy, Phys. Rev. A **60**, R13 (1999).
[15] A. T. Stelbovics, Phys. Rev. Lett. **83**, 1570 (1999).
[16] C. W. McCurdy, D. A. Horner, and T. N. Rescigno, Phys. Rev. A **65**, 042714 (2002).
[17] P. L. Bartlett and A. T. Stelbovics, Phys. Rev. A **69**, 022703 (2004).
[18] A. L. Frapiccini, J. M. Randazzo, G. Gasaneo, and F. D. Colavecchia, J. Phys. B **43**, 101001 (2010).
[19] M. Draeger, G. Handke, W. Ihra, and H. Friedrich, Phys. Rev. A **50**, 3793 (1994).
[20] M. S. Pindzola, D. Mitnik, and F. Robicheaux, Phys. Rev. A **59**, 4390 (1999).
[21] C. Plottke, I. Bray, D. V. Fursa, and A. T. Stelbovics, Phys. Rev. A **65**, 032701 (2002).
[22] C. Plottke, P. Nicol, I. Bray, D. V. Fursa, and A. T. Stelbovics, J. Phys. B **37**, 3711 (2004).
[23] D. A. Horner, C. W. McCurdy, and T. N. Rescigno, Phys. Rev. A **71**, 010701(R) (2005).
[24] D. A. Horner, C. W. McCurdy, and T. N. Rescigno, Phys. Rev. A **71**, 012701 (2005).

[25] P. L. Bartlett and A. T. Stelbovics, Phys. Rev. A **81**, 022715 (2010).
[26] P. L. Bartlett and A. T. Stelbovics, Phys. Rev. A **81**, 022716 (2010).
[27] D. A. Konovalov, D. V. Fursa, and I. Bray, Phys. Rev. A **84**, 032707 (2011).
[28] D. V. Fursa and I. Bray, Phys. Rev. A **52**, 1279 (1995).
[29] W. C. Fon, K. P. Lim, K. Ratnavelu, and P. M. J. Sawey, Phys. Rev. A **50**, 4802 (1994).
[30] K. Bartschat, E. T. Hudson, M. P. Scott, P. G. Burke, and V. M. Burke, Phys. Rev. A **54**, R998 (1996).
[31] M. Stepanovic, M. Minic, D. Cvejanovic, J. Jureta, J. Kurepa, S. Cvejanovic, O. Zatsarinny, and K. Bartschat, J. Phys. B **39**, 1547 (2006).
[32] D. A. Konovalov and I. E. McCarthy, J. Phys. B **27**, L741 (1994).
[33] D. A. Konovalov and I. E. McCarthy, J. Phys. B **28**, L139 (1995).
[34] U. Fano, Phys. Rev. **140**, A67 (1965).
[35] I. Bray and A. T. Stelbovics, Phys. Rev. A **46**, 6995 (1992).
[36] E. J. Heller and H. A. Yamani, Phys. Rev. A **9**, 1201 (1974).
[37] J. Broad and W. Reinhardt, J. Phys. B **9**, 1491 (1976).
[38] *The complete Java source code used in this study is freely available for academic use from jmatrix.googlecode.com or a relevant link at www.dmitrykonovalov.org . .*
[39] D. A. Konovalov and I. Bray, Phys. Rev. A **82**, 022708 (2010).
[40] M. Abramowitz and I. A. Stegun, eds., *Handbook of Mathematical Functions* (Dover Publications, Mineola, NY, 1965).
[41] S. P. Goldman, Phys. Rev. Lett. **73**, 2547 (1994).
[42] E. T. Hudson, K. Bartschat, M. P. Scott, P. G. Burke, and V. M. Burke, J. Phys. B **29**, 5513 (1996).
[43] G. J. Schulz, Rev. Mod. Phys. **45**, 378 (1973).
[44] S. J. Buckman and C. W. Clark, Rev. Mod. Phys. **66**, 539 (1994).
[45] Y. K. Ho and Z.-C. Yan, Phys. Rev. A **59**, R2559 (1999).